Retrieving Middle-Infrared Reflectance Using Physical and Empirical Approaches: Implications for Burned Area Monitoring

Renata Libonati, Carlos C. DaCamara, José Miguel C. Pereira, and Leonardo F. Peres

***Abstract*—A systematic comparison is carried out between retrieved values of middle-infrared (MIR) reflectance by means of the complete radiative transfer equation (RTE) and the simplified algorithm proposed by Kaufman and Remer in 1994 (KR94). The added value to be expected when using RTE is assessed both within and beyond the region where KR94 produces usable estimates of MIR reflectance, paying special attention to their application for discriminating burned areas (BAs) in tropical environments, where KR94 is the most common approach. For large values of land surface temperature (LST) and solar zenith angle (SZA), the retrieval of MIR reflectance based either on RTE or KR94 is an ill-posed problem, i.e., small perturbations due to sensor noise and uncertainties in atmospheric profiles and LST may induce large errors in the retrieved values. It is found that the RTE approach leads to better estimates in virtually all cases, with the exception of high values of LST and SZA, where results from KR94 are also not usable. Impacts on BA discrimination were finally evaluated using Moderate Resolution Imaging Spectroradiometer imagery showing a large fire event in southern Brazil. Synthetic values were generated, assuming a hot tropical environment, and MIR reflectance was retrieved using the two approaches. Whereas retrieved values of MIR reflectance via KR94 did not allow an effective discrimination between burned and unburned areas, those obtained via RTE have shown to be usable for BA monitoring, opening good perspectives for successful applications in hot tropical environments.**

***Index Terms*—Burned-area (BA) monitoring, middle infrared, Moderate Resolution Imaging Spectroradiometer (MODIS), reflectance, tropical regions.**

I. Introduction

THE ABILITY of the reflectance of the middle-infrared (MIR) spectral band (around 3.5–3.9 μm) to efficiently detect burned areas (BAs) in a wide variety of ecosystems has been widely recognized (e.g., [1]–[4]) due to a number of reasons that are worth being recalled. First, MIR is largely unaffected by the presence of most aerosols [5], a feature that makes it particularly adequate for monitoring the land surface during fire episodes. Second, the MIR spectral region contains the water absorption band and is therefore very sensitive to the presence of liquid water. Burned surfaces, which are partially or totally devoid of green vegetation and present very dry soil surfaces (particularly shortly after the fire) will accordingly appear quite bright in this spectral range, in strong contrast with the very low reflectance that is displayed in the near infrared (NIR) [6]. Third, when visible reflectances are replaced by MIR ones, there is a considerable reduction of sensitivity to the atmosphere, particularly (but not exclusively) due to the effect of aerosols. It is therefore not surprising that the MIR/NIR bispectral space has shown to be more appropriate for BA discrimination than the traditional visible/NIR space [1]–[3], particularly when the reflective part of MIR is used instead of the normalized total radiance [7]. This issue was recently readdressed by the authors [8] who have developed a new coordinate system that allows an improved discrimination between vegetation and BA using MIR/NIR reflectances.

Retrieval of MIR reflectance implies solving the problem of separating MIR reflectance from the total signal, a difficult task (e.g., [9]–[12]) that implies having an appropriate knowledge of how measurements in the MIR band may be affected by perturbing factors [13], namely, those associated to atmospheric conditions (e.g., high moisture and smoke aerosols). A number of previous works (e.g., [1]–[3]), as well as the recent one by [8], have relied on the approximate method proposed by Kaufman and Remer [11], hereafter referred to as KR94, which is fast and easy to implement but may be insufficiently accurate under specific surface and atmospheric conditions. An assessment was made by Kaufman and Remer [14] on the limitations of retrieved MIR reflectance by means of KR94 when the method is applied to discriminate BA in the Amazon and Cerrado regions of Brazil. Results demonstrate that the quality of retrieved values may decrease significantly when the relative contribution of the thermal emitted component to the total signal exceeds a threshold of about 75%, a situation that is more likely to happen in the case of surfaces characterized by low values of MIR reflectance. Such is the case of vegetation, where the relative contribution of the solar component to the total MIR signal tends to be small, particularly when the surface is hot (i.e., in case of relatively high values of land surface temperature—LST) and when the solar signal is further weakened due to low sun elevation angles (i.e., high values of solar zenith angle—SZA). According to [14], in such conditions,

Manuscript received September 23, 2010; revised May 9, 2011; accepted June 11, 2011. Date of publication July 25, 2011; date of current version December 23, 2011. This work was supported in part by the Portuguese Science Foundation (FCT) through Project FLAIR (PTDC/AAC-AMB/104702/2008) and in part by the EU 7th Framework Program (FUME) under Contract 243888. The work of R. Libonati was supported in part by FCT under Grant SFRH/BD/21650/2005.

R. Libonati and C. C. DaCamara are with the Instituto Dom Luiz, University of Lisbon, 1749-016 Lisbon, Portugal.

J. M. C. Pereira is with the Forest Research Centre, School of Agriculture, Technical University of Lisbon, 1349-017 Lisbon, Portugal.

L. F. Peres is with the Department of Meteorology, Federal University of Rio de Janeiro, 21941-970 Rio de Janeiro, RJ, Brazil, and also with the Instituto Dom Luiz, Centro de Geofísica, University of Lisbon, 1749-016 Lisbon, Portugal.

Color versions of one or more of the figures in this paper are available online at http://ieeexplore.ieee.org.

Digital Object Identifier 10.1109/TGRS.2011.2160186

the errors are at least on the same order of magnitude as the reflectance to be retrieved and are considerably higher for large values of LST and SZA.

The aforementioned limitations of KR94 are particularly relevant in tropical environments, where high values of LST naturally dominate the scenes and where the presence of clouds implies relying on data at pixels illuminated by low values of SZA, a rather common situation when using data from sensors onboard polar orbiters [14]. In the case of the Moderate Resolution Imaging Spectroradiometer (MODIS) onboard Aqua and Terra, the authors [14] have shown that use of the KR94 algorithm in tropical environments may erroneously lead to retrieved values of vegetation reflectance on the order of those characteristic of charcoal, thus impairing the discrimination of BA. In this context, retrieving MIR reflectance by means of the complete radiative transfer equation (RTE) may offer a means to circumvent the problem or, at least, to improve the estimates provided by KR94 in the domain where this algorithm is applicable.

The main purpose of the present study is to carry out an in-depth study of retrieved MIR reflectance using the RTE approach with the aim of assessing the advantages and disadvantages of this method compared with KR94 when applied to MODIS imagery for BA discrimination. The physics of the problem is first discussed by paying special attention to the main sources of errors in the RTE approach, namely, those associated to the following: 1) the radiometric noise; 2) the uncertainty in the atmospheric profiles; and 3) the uncertainty in LST, namely, the one associated to the MODIS LST product (MOD11_L2). The accuracy of retrieved solutions is then evaluated by comparing results from the so-called "error case," where input data are contaminated by errors from the aforementioned sources against the baseline defined by the "error-free case" where deviations in retrieved values are entirely due to the model uncertainty. Finally, a comparison of retrieval errors in MIR reflectance using the RE approach versus KR94 is made and an assessment is performed on the respective impacts when using MIR reflectance for BA discrimination.

II. Methods and Data

A. Physics of the Problem

The top of the atmosphere (TOA) radiance measured by a sensor in the MIR region is a combination of reflective and thermal emissive components. In the case of clear-sky conditions, one may write the following energy balance equation:

$$L_{\mathrm{MIR}} = t_{\mathrm{MIR}}\rho_{\mathrm{MIR}}\frac{E_{0\mathrm{MIR}}}{\pi}\mu_0 + \tau_{\mathrm{MIR}}\varepsilon_{\mathrm{MIR}}B(\lambda_{\mathrm{MIR}}, T_S) + L_{\mathrm{atm,MIR}}\uparrow + \tau_{\mathrm{MIR}}\rho_{\mathrm{MIR}}\bar{L}_{\mathrm{MIR}}\downarrow + L_s \quad (1)$$

where $E_{0\mathrm{MIR}}$ is the solar irradiance incident on TOA, $B(\lambda_{\mathrm{MIR}}, T_S)$ is the emitted radiance given by Planck's function for the surface temperature T_S and the central wavelength λ_{MIR}, $L_{\mathrm{atm,MIR}}\uparrow$ is the atmospheric upward emission, $\overline{L}_{\mathrm{MIR}}\downarrow$ is the hemispherically averaged downward radiance that includes both solar diffuse radiation and atmospheric emitted radiation, L_S is the scattered solar radiation, ρ_{MIR} is the surface reflectance, $\varepsilon_{\mathrm{MIR}}$ is the surface emissivity, μ_0 is the cosine of the SZA, t_{MIR} is the two-way atmospheric transmittance, and τ_{MIR} is the one-way atmospheric transmittance. It may be noted that, in (1), the transmittances corresponding to the surface emittance, solar diffuse radiation, and atmospheric downward emitted radiance are assumed to be equal and represented by τ_{MIR}. This assumption is due to the fact that the set of simulated radiances was produced using the Moderate Spectral Resolution Atmospheric Transmittance and Radiance Code 4 (MODTRAN-4) [15], where the three transmission functions are assumed to be equal at wavenumber intervals of 1 cm^{-1}. Moreover, the surface is considered to be Lambertian, i.e., the surface reflectance is assumed to be isotropic. Within the 3–14-μm range, the Lambertian surface approximation does not introduce a significant error in the terms concerning the surface-reflected diffuse solar and surface-reflected atmospheric downward thermal irradiances, since atmospheric radiative transfer simulations show that, in clear-sky conditions, the surface-reflected diffuse solar irradiance term is much smaller than the surface-reflected solar beam term and the surface-reflected atmospheric downward thermal irradiance term is smaller than the surface thermal emission [16].

Since the Earth's surface is opaque and assuming that it behaves as a Lambertian emitter–reflector, the reflectance and emissivity at the surface may be related as $\rho = 1 - \varepsilon$. Thus, by neglecting the atmospheric scattering term L_S, the solution of (1) is given by

$$\rho_{\mathrm{MIR}} = \frac{L_{\mathrm{MIR}} - \tau_{\mathrm{MIR}}B(\lambda_{\mathrm{MIR}}, T_S) - L_{\mathrm{atm,MIR}}\uparrow}{t_{\mathrm{MIR}}\frac{E_{0\mathrm{MIR}}}{\pi}\mu_0 - \tau_{\mathrm{MIR}}B(\lambda_{\mathrm{MIR}}, T_S) + \tau_{\mathrm{MIR}}\bar{L}_{\mathrm{MIR}}\downarrow}. \quad (2)$$

It is worth noting that the effects of atmospheric scattering were neglected in (2), an assumption that is justified by comparing the contributions to the MIR signal due to surface emission, surface reflection, atmospheric emission, and atmospheric scattering. Fig. 1 shows box–whisker plots of such contributions as derived from a set of more than 2700 MODTRAN-4 simulations of a tropical environment covering a large number of viewing and solar geometries and a wide range of boundary conditions. Details about the simulations are provided in Section II-B. The tropical atmospheric profile was also progressively contaminated with smoke aerosol. The lower and upper lines of each box refer to the 25th and 75th percentiles of the sample, whereas the line inside the box is the sample median. The top (bottom) of the upper (lower) whisker indicates the maximum (minimum) value of the set of simulations. It may be noted that the contribution of atmospheric scattering for the total signal ranges from 0.001% (for an atmosphere free from aerosol) to 1% (for an atmosphere contaminated with heavy biomass burning aerosol) and is orders of magnitude smaller than the other terms. Accordingly, even in the presence of heavy smoke layers, the scattered radiance around 3.9 μm is very small when compared with the other terms and may be neglected without affecting the accuracy of (1).

Equation (1) defines the so-called forward (direct) problem, i.e., the surface parameter ρ_{MIR} is known and the radiance is then evaluated through the RTE, which describes the various physical processes responsible for making the radiance reach the sensor. In turn, the so-called inverse problem is defined by

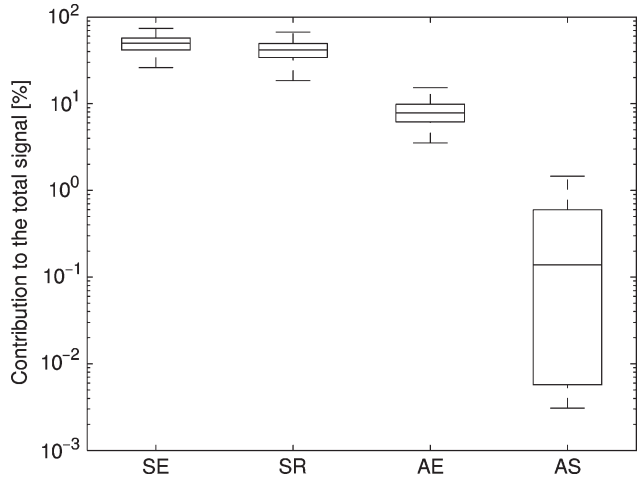

Fig. 1. Contribution to the MIR signal due to (SE) surface emission, (SR) surface reflection, (AE) atmospheric emission, and (AS) atmospheric scattering for a large set of viewing and solar geometries and boundary conditions and considering a tropical atmospheric profile that is progressively contaminated with smoke aerosol.

(2) and corresponds to the retrieval of the surface reflectance from the measured radiance. This procedure involves the direct evaluation of all components of the MIR signal by means of a radiative transfer model. Aside from requiring substantial computational means, the operational use of the RTE is limited by the need of quantitative information on the following: 1) atmospheric conditions, mainly humidity and temperature profiles, which are required to perform the atmospheric corrections, and 2) LST, which is required as a boundary condition.

The aforementioned limitations led to the development of simpler methods, like the one proposed by KR94, which require neither direct knowledge of atmospheric conditions nor a radiative transfer model. The approach is based on [17] and [18], which pointed out the existence of a mutual compensation between attenuation and thermal emission terms, such that both atmospheric transmittances (i.e., t_{MIR} and τ_{MIR}) may be assumed as equal to unity and both the atmospheric downward and upward thermal emission terms may be neglected. As shown in [14], the validity of these assumptions for surface and atmospheric conditions associated to dense dark vegetation areas in midlatitude environments may be justified both on mathematical and physical grounds. This is first done by means of algebraic manipulation followed by simplification of terms of (2) and then by checking the performed simplifications using typical values of the relevant terms of (2), leading to the following simplified expression:

$$\rho_{\mathrm{MIR}} = \frac{L_{\mathrm{MIR}} - B(\lambda_{\mathrm{MIR}}, T_S)}{\frac{E_{0\mathrm{MIR}}}{\pi}\mu_0 - B(\lambda_{\mathrm{MIR}}, T_S)}. \tag{3}$$

B. Radiative Transfer Simulations

The estimation of the error associated with MIR reflectance as retrieved by using either RTE, i.e., (2), or the KR94 method, i.e., (3), will be performed based on a large number of simulated TOA radiances, as generated by means of MODTRAN-4. In order to cover MODIS channels 20 and 31, the simulations will be performed in the spectral ranges of 3.62–3.97 and 10–12 μm.

The following cases will be considered, which encompass a large set of observation conditions.

1) *Atmospheric Temperature and Humidity Profiles*: The database relies upon standard profiles with respect to three geographical–seasonal model atmospheres stored in MODTRAN-4, namely, Midlatitude Winter (MLW), Midlatitude Summer (MLS), and Tropical (TRO). The three standard atmospheres are tabulated at 36 levels in terms of temperature, humidity, and pressure and cover a wide range of thermal and moisture conditions, the 2-m air temperature ranging from 272.2 to 299.7 K and the total water vapour ranging from 0.85 to 4.11 g $\cdot$ cm^{-2}.
2) *LST*: The assigned LST values are defined as departures from the 2-m air temperature of each profile, varying from T_{atm} to $T_{\mathrm{atm}} + 30.0$ K in steps of 1.0 K, totalizing 31 distinct boundary conditions.
3) *LSE/reflectance*: Two types of surface cover are considered, namely, burned and unburned. Following [14], both surface types were assumed homogeneous and Lambertian and were characterized based on available spectral data for charcoal and vegetation. A value of 0.24 (0.03) was accordingly prescribed for the MIR reflectance for the burned (unburned) types of surface cover. These values were obtained via the Band Equivalent Reflectance for MODIS channel 20 [19], [20] which was applied to a data set of four (25) considered types of charcoal (vegetation) spectra. Details may be found in [14].
4) *Sun-view geometry*: The sun-view geometry consists of 31 values of SZA, from 0° to 60° in steps of 2° and three values of view zenith angles (VZAs), i.e., 0°, 30°, and 60°, respectively.

C. Sources of Errors in the Retrieval of MIR Reflectance

Aside from the errors inherent to the inversion procedure and those introduced by the adopted approximations, the accuracy of (2) will depend essentially on the following three sources of error, namely: 1) the error due to instrument performance, which is quantified by the radiometric noise; 2) the uncertainties on the atmospheric profile, which are usually due to the errors in temperature and humidity profiles; and 3) the error due to uncertainties in the retrieval of the LST. Contribution of each source of error will be analyzed separately in the following sections.

1) Radiometric Noise: The radiance measured by a sensor onboard a satellite is affected by an inherent uncertainty due to electronic devices involved in the construction of the sensor [21]. Levels of noise to be introduced into the MODIS channel were based on the noise-equivalent temperature (NEΔT) at 300 K of channel 20 (0.05 K), which were converted to the respective noise-equivalent radiance (NEΔL). The radiance sensitivity of channel 20 to small changes in temperature is shown in Fig. 2.

Randomly generated perturbations were then added to the simulated TOA radiances which were assumed as normally distributed around zero mean and with standard deviations (SDs) equal to the respective MODIS channel NEΔL. As shown in Fig. 3, a set of 1000 random perturbations were generated in order to ensure a statistically significant result.

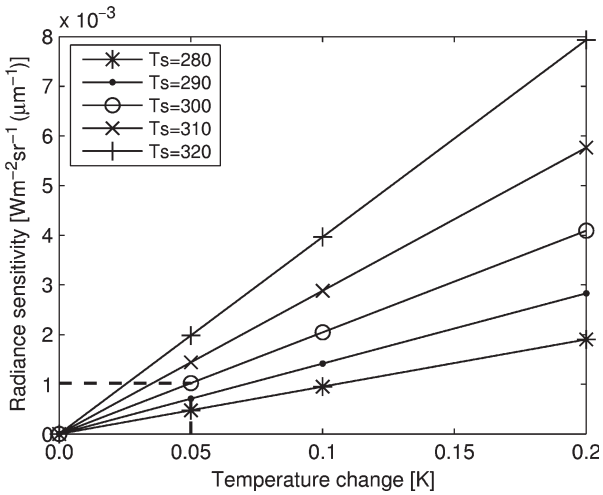

Fig. 2. Sensitivity of MODIS channel 20 to small changes in temperature. The dashed line indicates the values of NEΔT and NEΔL.

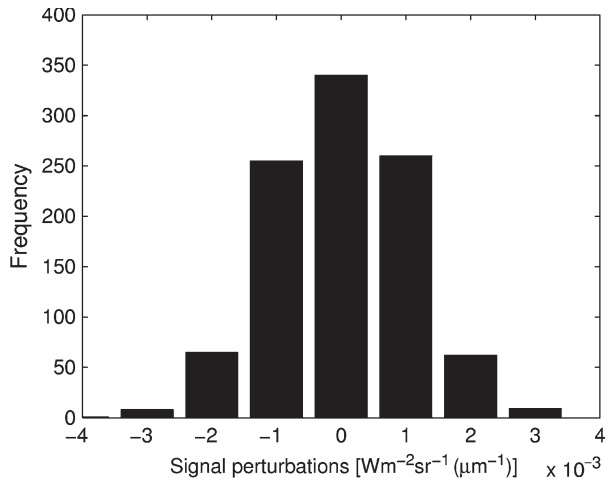

Fig. 3. Frequency histogram of the satellite radiance perturbations for MODIS channel 20.

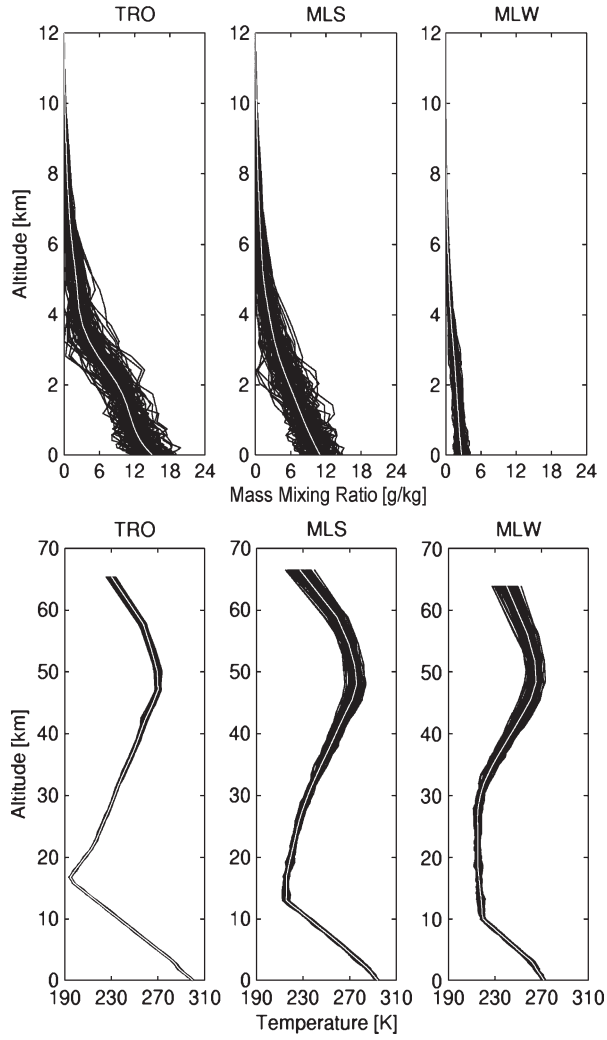

Fig. 4. Comparison between the (black curves) perturbed profiles and (white curves) respective reference profile of (upper panels) water-vapor mass mixing ratio and (lower panels) temperature. Adapted from [24].

2) Uncertainty in Atmospheric Profiles: The effects of uncertainties on the humidity and temperature profiles may be analyzed by comparing TOA radiation for a given perturbed profile with the radiance for the reference profile. Because the results will depend on the reference (nonperturbed) profile, the experiment adopts the three standard atmospheres stored at MODTRAN-4, namely, TRO, MLS, and MLW.

A possible way to take into account the errors in the atmospheric profiles might consist in perturbing each atmospheric profile level with values randomly taken from a normal distribution of zero mean and an SD characteristic of the uncertainty. In this case, perturbations on temperature and water vapor are assumed to be independent from each other and values of both quantities at a given level are also taken as independent from those at the other levels. An extreme opposite procedure would be considering the perturbations to be perfectly correlated, e.g., by using perturbed profiles that are offset by given amounts [22]. Since, in our case, we intend to perform a sensitivity study reflecting more realistic situations, we followed [23], where the three standard profiles were perturbed with values based on the background error covariance matrix used in the assimilation schemes of the Global Circulation Model operated at the European Centre for Medium-Range Weather Forecasts (ECMWF) [24]. The covariance coefficients were computed statistically using the method developed by the National Centers for Environmental Prediction that is based on 24/48-h forecast differences of the ECMWF model and the so-called background. The background is a short-range forecast which has been started from the analysis at the previous assimilation cycle and is used, in conjunction with a set of observations, to help in finding the new analysis state. Unlike the MODTRAN-4 standard profiles that are tabulated at 36 levels, the ECMWF model prognostic values of temperature and specific humidity are currently represented on a vertical grid with 60 levels (from TOA to the surface). The MLS, MLW, and TRO profiles were therefore interpolated to the 60 pressure-level grids and only then were the perturbations imposed on the three standard atmospheres. Fig. 4 allows a visual comparison between the perturbed profiles and the respective reference profile of water-vapor mass mixing ratio and the one of temperature.

Although it might seem obvious, at first sight, to adopt the error associated with the MODIS Atmospheric Profile product (since it is the main sensor considered in the present study), the use of the ECWMF background error covariance matrix

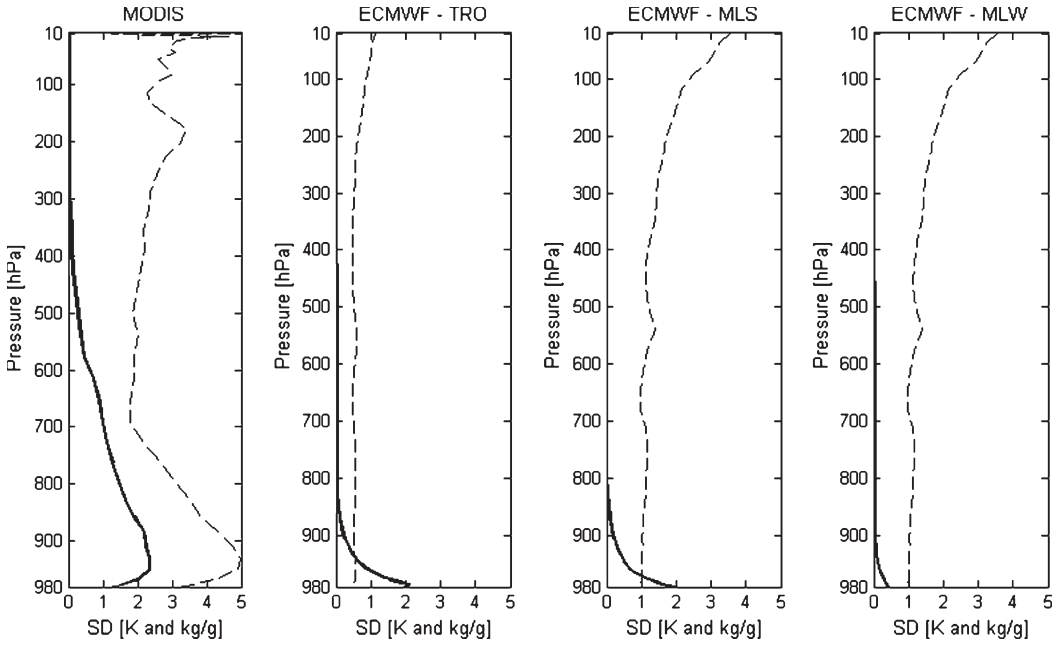

Fig. 5. SD of the MODIS and the three ECMWF (TRO, MLS, and MLW) SD profiles of (solid curves) mass mixing ratio and (dashed curves) temperature.

is preferable because it allows generating sets of perturbed profiles of temperature and humidity based on the reference TRO, MLS, and MLW profiles. The set of imposed errors due to uncertainties on atmospheric information therefore corresponds to a specific and predefined standard profile/atmospheric condition. On the other hand, information about accuracy of the MODIS product is based on the comparison between collocated MODIS profile retrievals and the so-called best estimated profiles [25] at the Southern Great Plains Atmospheric Radiation Measurement site for 80 clear-sky Aqua cases between October 2002 and August 2005. The best estimated profiles of the atmospheric state are an ensemble of temperature and moisture profiles generated from two radiosondes launched within 2 h of the Aqua satellite overpass times. The use of the ECMWF background error covariance matrix therefore provides uncertainty information that is more realistic for each standard profile than that from the MODIS product. Moreover, and as shown in Fig. 5, the computed SDs of the mass mixing ratio (solid curves) and temperature (dashed curve) errors using the ECMWF background error covariance matrix present lower values than the SDs from the MODIS Atmospheric Profile product. Perturbing the three standard profiles by using the former type of errors may be viewed as adopting the most favorable conditions when assessing the effect of the atmospheric profile source of error on the retrieval of MIR reflectance.

The imposed perturbations on the atmospheric profiles translate into uncertainties on the atmospheric parameters in (2), namely, the one-way total atmospheric transmittance, the two-way total atmospheric transmittance, the upward atmospheric radiance, and the downward atmospheric radiance. Statistical distributions of the perturbations on the atmospheric parameters are shown in Figs. 6–8, respectively.

3) Uncertainty in Surface Temperature: In order to take into account the sensitivity of the MIR reflectance retrieval to the LST, radiative transfer calculations are first performed for the standard profiles, and then, errors associated to inaccuracies in

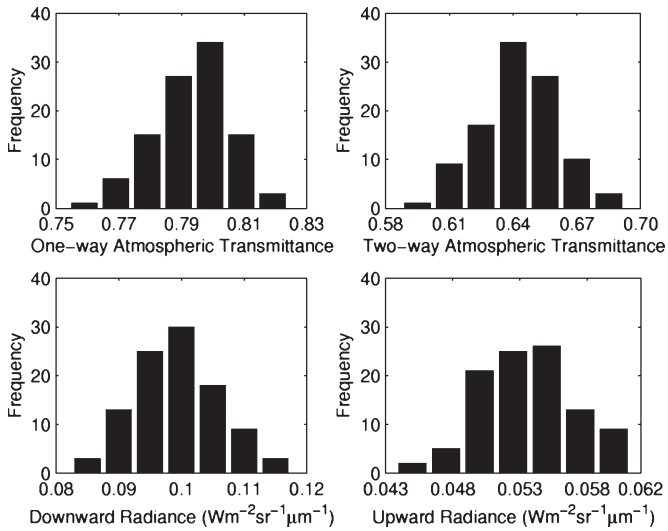

Fig. 6. Distributions of the perturbed atmospheric parameters, namely, one-way total atmospheric transmittance, two-way total atmospheric transmittance, atmospheric upward radiance, and atmospheric downward radiance, with respect to MODIS channel 20 for TRO standard atmosphere.

LST are introduced into (2). The errors are generated based on the accuracy specification for MODIS LST (1 K) at 1-km resolution under clear-sky conditions [26]. The generated errors are normally distributed around zero mean and with SDs equal to the respective accuracy specification for MODIS LST. A set of 1000 random perturbations (Fig. 9) was again generated in order to guarantee a statistically significant result.

III. Analysis and Results

A. Error-Free Case

The accuracy of the solutions to the inverse problem was assessed based on the evaluation of the retrieval errors, defined as the absolute differences between retrieved values of MIR reflectance by means of (2) and the corresponding values

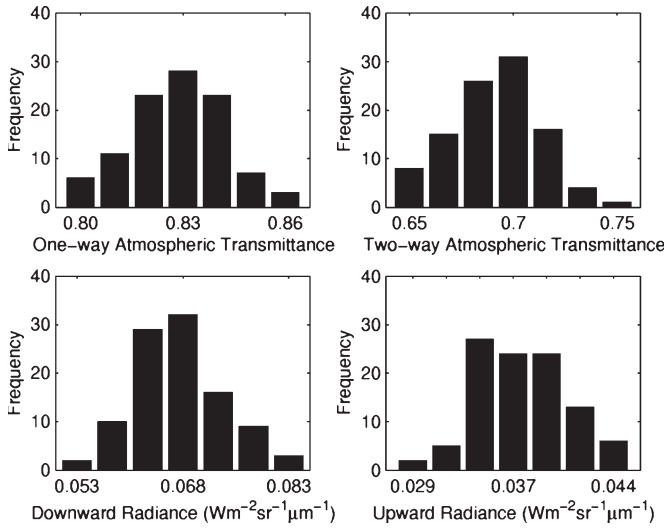

Fig. 7. Same as that in Fig. 6 but for MLS standard atmosphere.

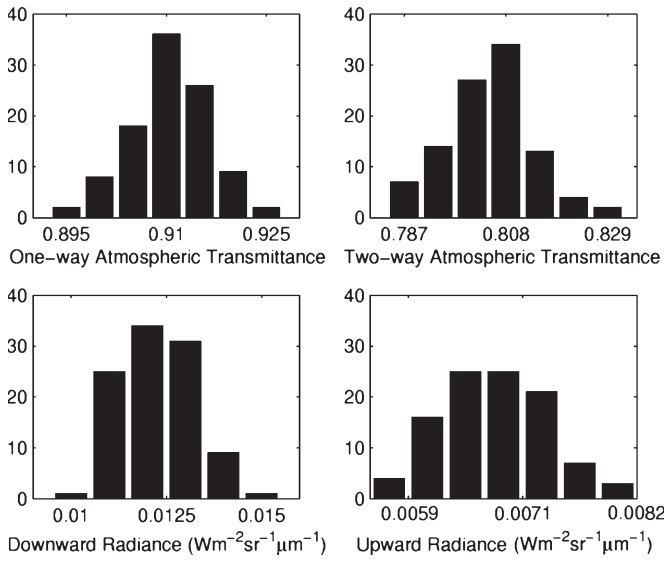

Fig. 8. Same as that in Fig. 6 but for MLW standard atmosphere.

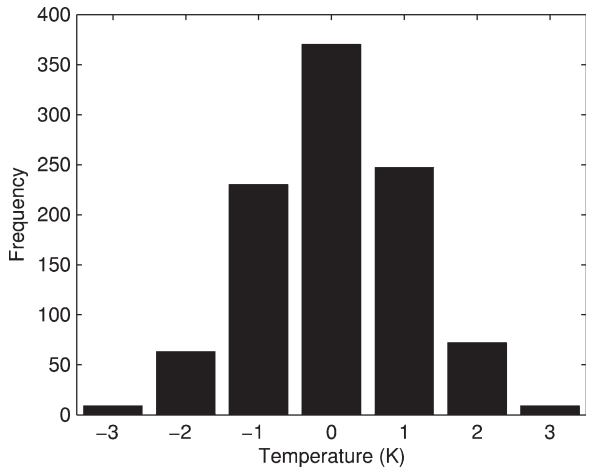

Fig. 9. Frequency histogram of the errors in LST.

prescribed as input to MODTRAN-4. Although actual retrieved values of MIR reflectance are affected by measurement uncertainties, the assessment was initially carried out under the assumption of error-free input data, implying that the errors in the MIR reflectance are entirely due to the model uncertainty. The reason for this first step is that it allows the identification of the problems that are exclusively due to the inversion procedure under the prescribed large set of observation conditions that was described in the previous section. Such approach, usually referred to in the literature as inverse method parameter sensitivity [27], is particularly adequate in our study, not only because it allows the evaluation of the contribution to the retrieval error due to the inverse method but also particularly because it helps establishing a baseline that reveals pitfalls that are likely to occur when retrieving MIR reflectance from real data.

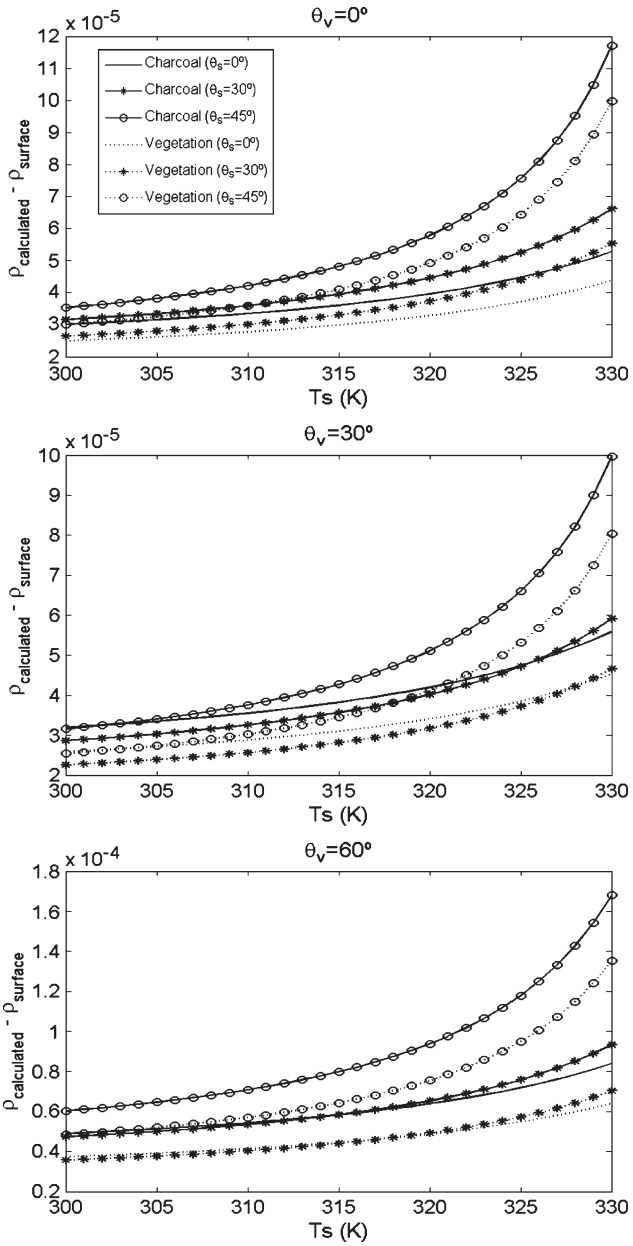

Fig. 10. Dependence on LST of the accuracy in the retrieval of MIR reflectance for (full lines) charcoal and (dashed lines) pine tree when using (2) in the case of the TRO profile and with (top, middle, and bottom panels) three prescribed values of VZA and (three pairs of curves in each panel) three values of SZA.

Fig. 10 summarizes the accuracy of results in the case of the TRO profile when using (2) to retrieve MIR reflectance

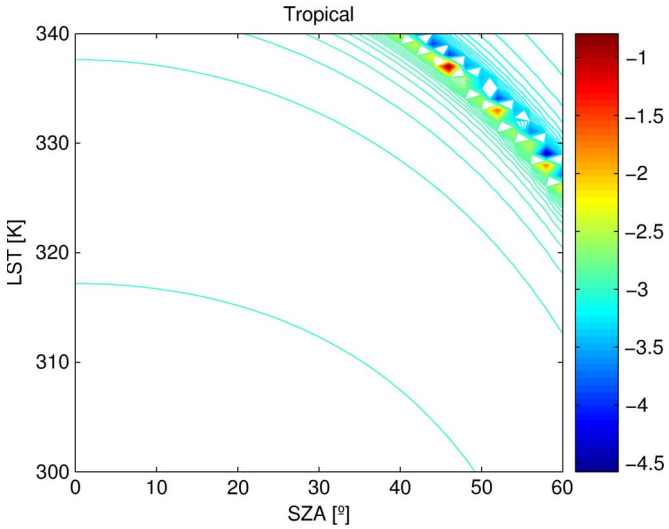

Fig. 11. Dependence of the logarithm of retrieval error on LST and SZA for TRO profile.

for charcoal (full lines) and pine tree (dashed lines). The three panels respect three prescribed values of VZA, and the three pairs of curves refer to three prescribed values of SZA. As expected, there is a slight degradation in MIR reflectance retrieval with increasing VZA, indicating a weak dependence of the MIR region on view angle variations, both for bright and dark surfaces. These results are in agreement with [4] and [28]. The deviation in MIR reflectance with SZA (from 0° to 45°) is weak for low values of LST, and as the LST increases, the angular deviations with SZA become more prominent. Although not shown, similar results were found for MLS and MLW profiles.

The dependence of retrieval errors in MIR reflectance on both LST and SZA is shown in Fig. 11, where retrieval errors are represented on a logarithmic scale in order to enhance the error variation. Large and abrupt fluctuations in the retrieval error may be observed for different combinations of SZA and LST along a curved stripe at the upper right corner of Fig. 11. For instance, the logarithm of the retrieval error reaches the value of -0.74, which corresponds to the pair SZA $= 46°$ and LST $= 337$ K. This value of retrieval error is equivalent to a relative error around 25%, and it may be observed that, for the same value of LST but with SZA $= 24°$, the relative error is as low as 0.38%. The obtained pattern along the curved stripe strongly suggests that the solution does not depend continuously on the data and is typical of ill-conditioning [29].

Further evidence of ill-conditioning behavior is shown in Fig. 12, which presents the dependence on surface temperature of errors in the retrieval of charcoal MIR reflectance in the case of the TRO (left panel), MLS (middle panel), and MLW (right panel) profiles. Four values of SZA are considered (which include the angle of 60°), and the observations are assumed to be performed at nadir, corresponding to the most favorable view condition. It is worth noting that, in case of sufficiently high values of LST, critical regions where the problem is ill-posed occur for all considered types of atmospheres. Nevertheless, for MLW, the critical region is located well beyond the range of observed/physical LST values in temperate regions. In the case of midlatitudes (MLW and MLS), and excluding the case of very low sun elevations, large retrieval errors of reflectance are also not to be expected.

The problem of MIR reflectance retrieval is therefore very likely to be ill-conditioned for ranges of LST and SZA typically observed over tropical regions. Fig. 13 shows the behavior of each term of (2), with the exception of that concerning the total radiance L_{MIR} for four values of SZA, namely, 0°, 20°, 40°, and 60°. For instance, considering SZA between 40° and 60°, the curve corresponding to the term $\tau_{\mathrm{MIR}} B(\lambda_{\mathrm{MIR}}, T_S)$ crosses that corresponding to the term $t_{\mathrm{MIR}}(E_{0\mathrm{MIR}}/\pi)\mu_0$ around 325 K. As temperature rises, the former term increases up to the magnitude of the latter term (which decreases with the increase of SZA) and the denominator of (2) tends to zero, inducing large variations in the solution. However, the problem will also be ill-conditioned for all regions where the curves are close enough, and it will not restrict to the single point where the curves cross each other. In addition (and as shown in Fig. 13 for SZA $= 0°, 20°, 40°,$ and 60°), the curve representing the term $\tau_{\mathrm{MIR}} B(\lambda_{\mathrm{MIR}}, T_S)$ will cross an infinite number of curves $t_{\mathrm{MIR}}(E_{0\mathrm{MIR}}/\pi)\mu_0$ resulting in peaks of error (positive and negative), as those shown in Figs. 11 and 12.

At first sight, it may be argued that the obtained magnitude of retrieval errors is not large enough to prevent discrimination between charcoal and vegetation. However, the analysis performed refers to the error-free input data case, and therefore, the other sources of error were not taken into account. In fact, when using real data, the inversion problem will certainly become more difficult to solve because the errors related to both sensor performance and the meteorological parameters are usually much larger than the error due to model uncertainties. This aspect will be dealt with in the next section.

B. Error Case

The performance of the RTE will be now evaluated based on the solution to the inversion problem [27], as given by (2). Simulations of TOA radiance at MODIS channel 20, as well as the imposed perturbations (i.e., noise in the satellite radiances and measurement errors in the atmospheric profiles as well as in LST), were generated as described in the previous section.

Figs. 14–19 summarize the errors in MIR reflectance using (2), as obtained from each set of imposed perturbations on the considered atmospheric profiles. Figs. 14–16 (Figs. 17–19) pertain to charcoal (vegetated) surfaces, respectively, for TRO, MLS, and MLW profiles. Each figure refers to a prescribed set of four values of SZA (0°, 30°, 45°, and 60°), and in each panel, the contribution of noise and errors in profiles and LST is shown for three values of VZA (0°, 30°, and 60°). For all atmospheres, the contribution of instrumental error is not represented because it is negligible compared with the other sources of error. The same happens with KR94, and the negligible impact of instrumental noise (when using either RTE or KR94) is understandable, taking into account the low sensitivity of the MODIS channel 20 radiance to changes in temperature (Fig. 2).

In the case of charcoal surfaces and for SZA between 0° and 45°, the measurement errors in LST and the inaccuracies in atmospheric profiles have impacts of comparable magnitude.

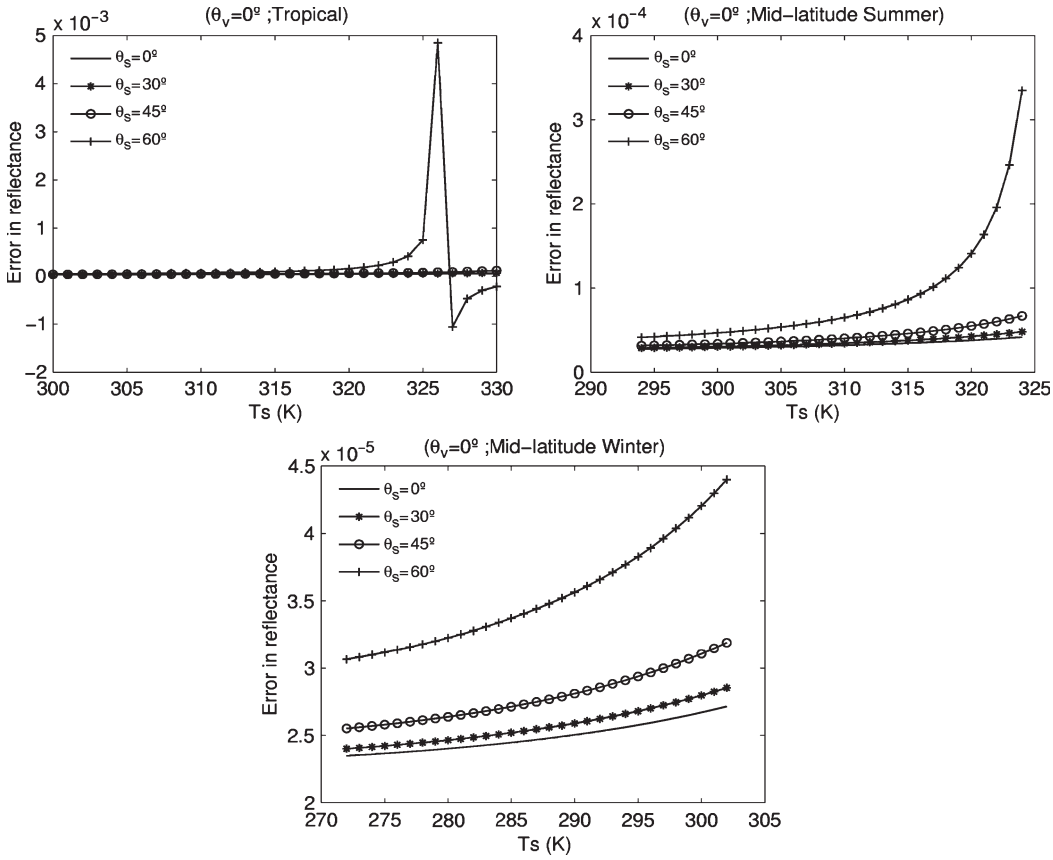

Fig. 12. Dependence on LST of errors in the retrieval of charcoal MIR reflectance in the case of TRO, MLS, and MLW for nadir view and for four values of SZA.

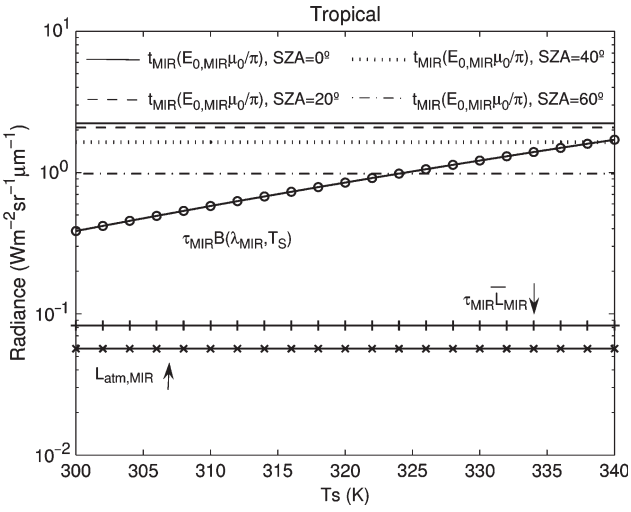

Fig. 13. Dependence on LST of the different terms of (2). The term $\tau_{\mathrm{MIR}} B(\lambda_{\mathrm{MIR}}, T_S)$ is represented for four values of SZA.

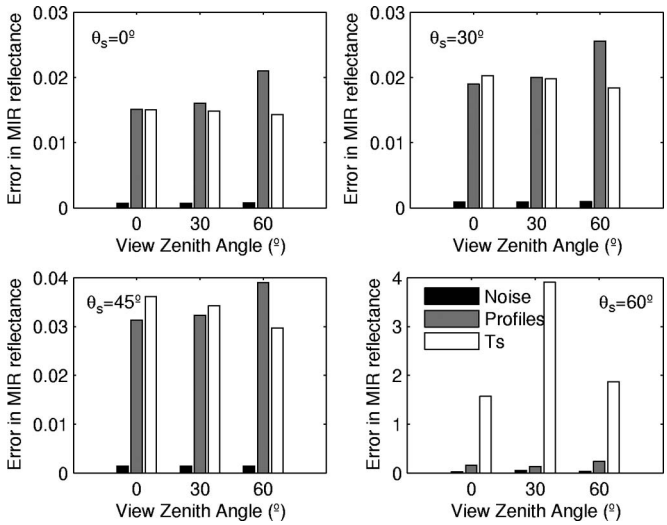

Fig. 14. Retrieval error in charcoal MIR reflectance when using (2) as obtained from each set of imposed perturbations on the TRO profile for four prescribed values of SZA (0°, 30°, 45°, and 60°) and three prescribed values of VZA (0°, 30°, and 60°).

In contrast to charcoal surfaces, inaccuracies in LST are the most important source of error in the case of vegetation. The impact of errors of all sources is also more pronounced for the TRO profile than for MLS and MLW. For instance, in the case of TRO, for charcoal, and for SZA between 0° and 45°, the maximum error due to measurement inaccuracies in the atmospheric profiles is around 0.04, whereas the maximum error due to measurement inaccuracies in LST is around 0.035, with mean values around 0.02. In the case of TRO and vegetation, the maximum error due to measurement inaccuracies in the atmospheric profiles is around 0.035, while the maximum error due to measurement inaccuracies in LST is around 0.05.

In the case of low sun elevations (SZA equal to 60°), the ill-conditioned behavior may be observed, again, to be in good agreement with the results obtained in [14] for KR94, and it may be further noted that the measurement errors in LST become the most important source of error.

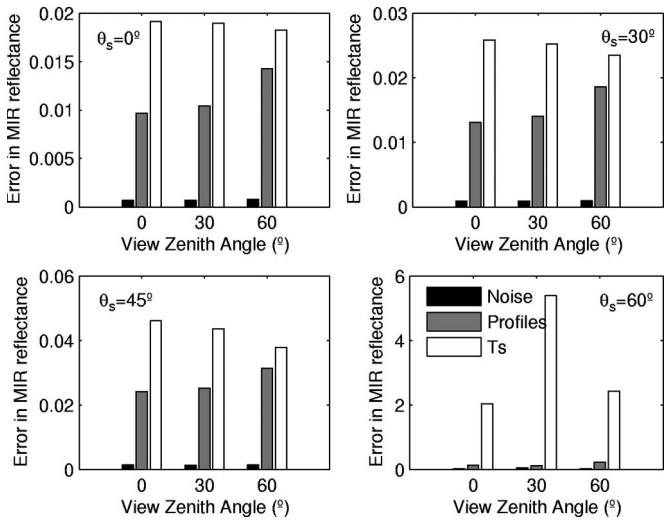

Fig. 15. Same as that in Fig. 14 but for a vegetated surface.

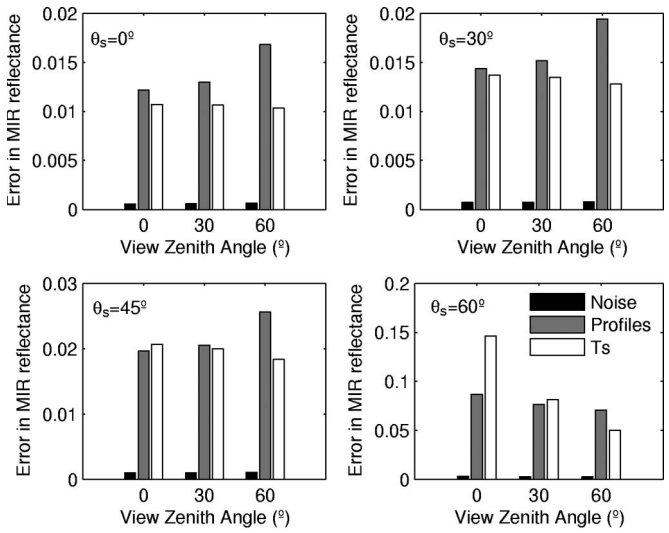

Fig. 16. Same as that in Fig. 14 but for the MLS profile.

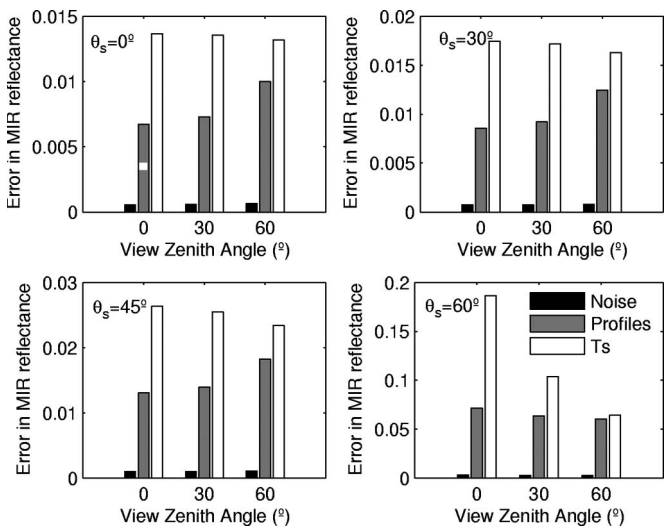

Fig. 17. Same as that in Fig. 15 but for the MLS profile.

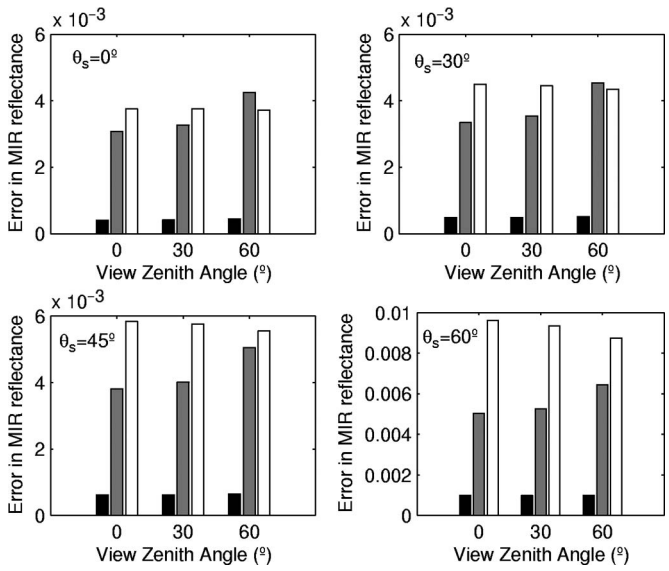

Fig. 18. Same as that in Fig. 14 but for the MLW profile.

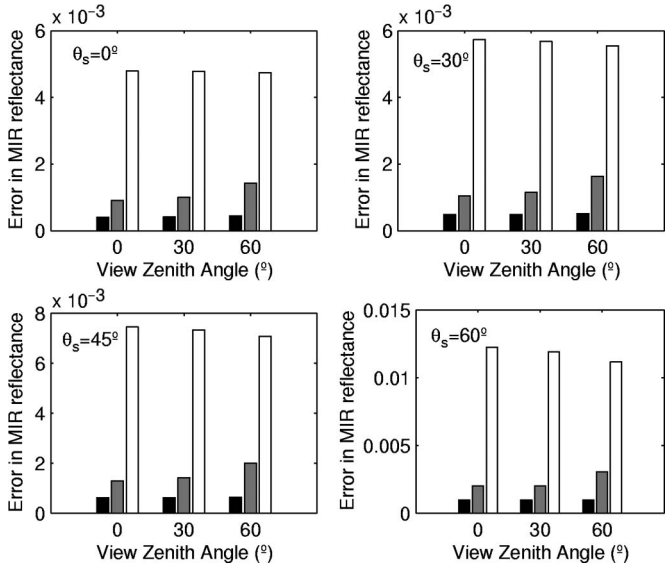

Fig. 19. Same as that in Fig. 15 but for the MLW profile.

Fig. 20 shows the obtained dependence of retrieval errors on LST and SZA for an offset of $+1$ K in LST. The value of the offset was chosen based on the goal that was set for the accuracy of the MODIS LST algorithm [15]. The ill-conditioning behavior that is present in Figs. 14–19 for SZA equal to 60° may now be observed in a continuous way. As expected, retrieval errors present similar fluctuations to those previously obtained with the sensitivity experiment corresponding to the error-free input data case (Fig. 11). When compared with that in Fig. 11, the offset of $+1$ K in LST greatly amplifies the retrieval errors (as indicated by the statistics derived from results in Figs. 14–19), leading to unrealistic physical solutions in some of the simulations. For instance, relative errors may reach $7.0 \times 10^4\%$ for SZA $= 46^\circ$ and LST $= 336$ K. It is also worth stressing that Fig. 20 may be useful to defining a critical region in the space SZA versus LST where the solution does

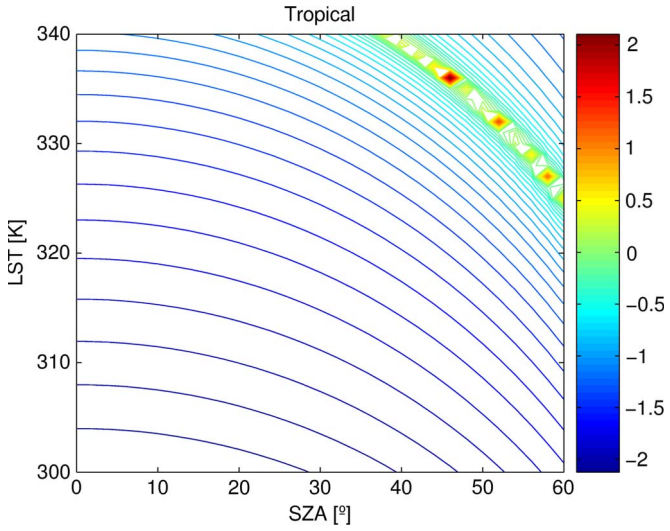

Fig. 20. Same as that in Fig. 11 but for an offset of +1 K in LST.

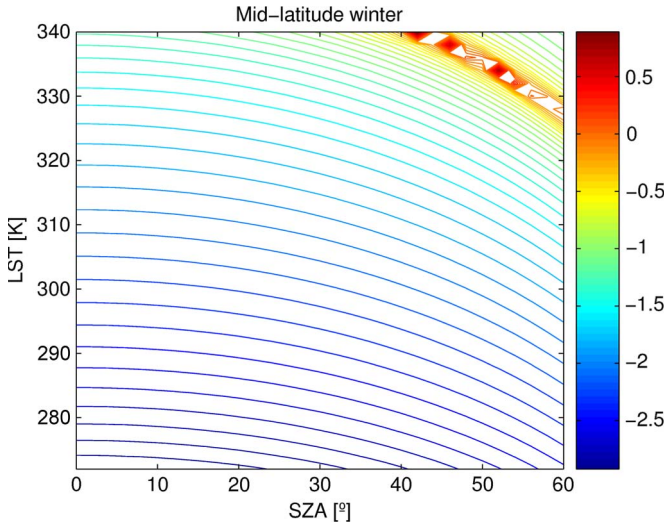

Fig. 21. Same as that in Fig. 20 but for the MLW atmosphere.

not depend continuously on the data and, therefore, where the retrieval of MIR reflectance is severely impaired.

Critical regions where the problem is ill-posed also occur for other types of atmospheres in case of sufficiently high values of LST. Nevertheless, and as already found in the error-free case, for midlatitude winter atmospheres (Fig. 21), the critical region is located well beyond the range of observed/physical LST values in temperate regions and, except for very low sun elevations, large retrieval errors of reflectance are not to be expected.

C. Total MIR Reflectance Error

Assuming that the three retained sources of errors are independent, the total error in MIR reflectance using the RTE (2) is given by

$$\delta\rho = \left[(\delta\rho_a)^2 + (\delta\rho_T)^2 + (\delta\rho_n)^2\right]^{1/2} \tag{4}$$

where $\delta\rho_a$, $\delta\rho_T$, and $\delta\rho_n$ are the errors due to the atmospheric correction, LST uncertainty, and radiometric noise,

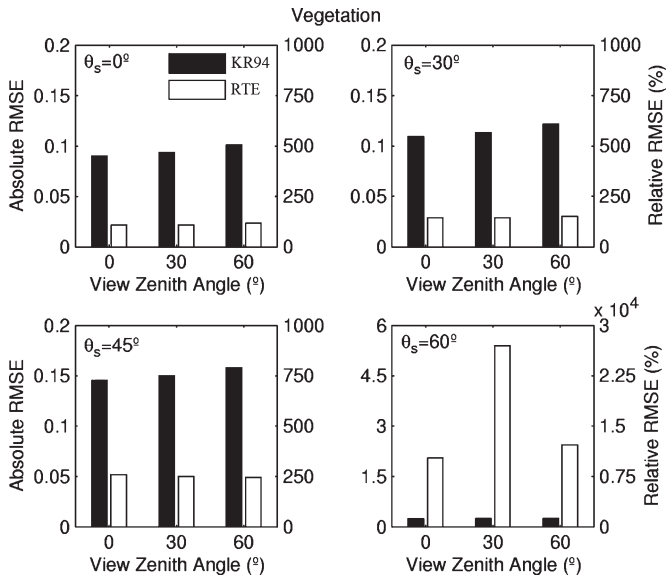

Fig. 22. Comparison between the total errors when using KR94 and RTE in the case of TRO and for vegetation.

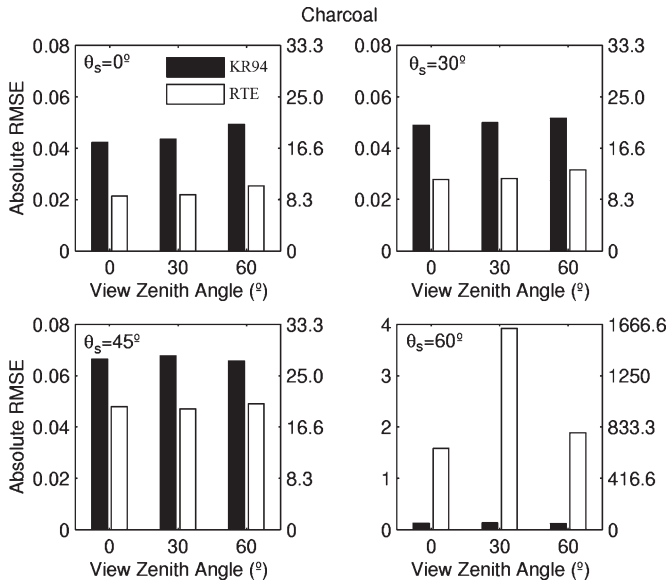

Fig. 23. Same as that in Fig. 22 but for charcoal.

respectively, as discussed in the previous section. Figs. 22–27 show the total error in MIR reflectance, for vegetation (MIR reflectance around 0.03) and charcoal (MIR reflectance around 0.24), as obtained throughout RTE and KR94, for each angle considered in this study and in the case of the TRO, MLS, and MLW profiles.

As found in [14], MIR reflectance errors for charcoal are generally lower than reflectance errors for vegetation, and the same is valid for dry and moist atmospheres. When comparing the MLW and the TRO, given the much lower values of moisture of the former, together with colder temperatures, the perturbation effects exerted by the MLW atmosphere on the retrieval of MIR reflectance is much smaller when using either KR94 or RTE. Restricting to results when the SZA lies between 0° and 45°, the maximum values of the relative errors vary from 750% (KR94—vegetation) to 30% (KR94—charcoal) and from

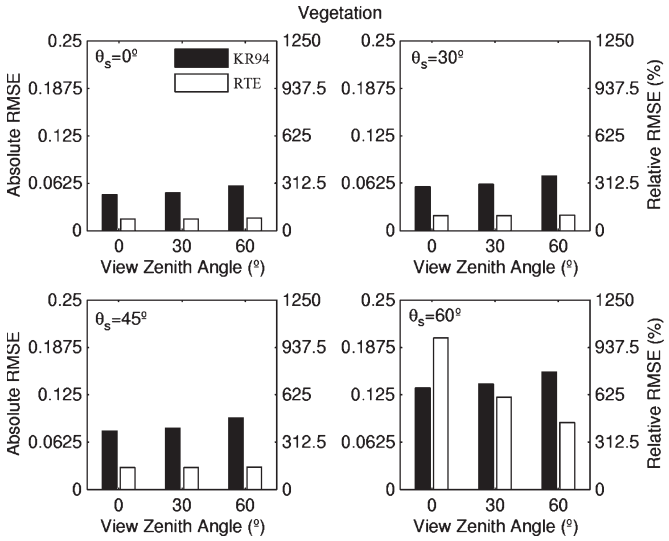

Fig. 24. Same as that in Fig. 22 but for MLS.

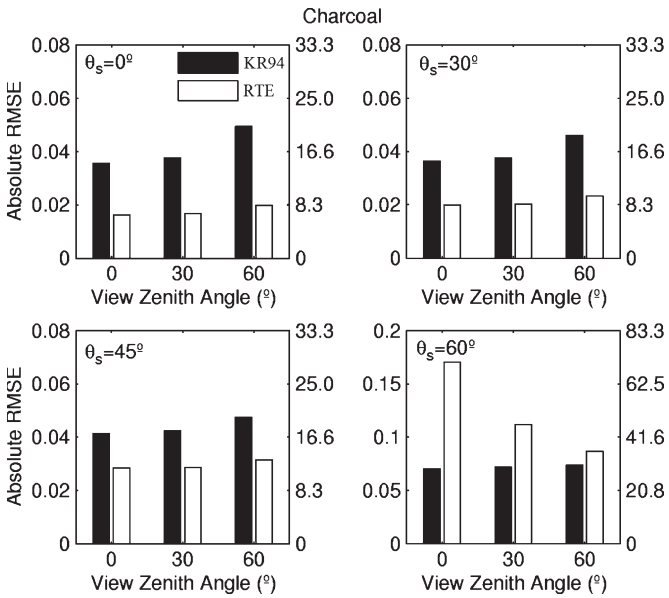

Fig. 25. Same as that in Fig. 24 but for charcoal.

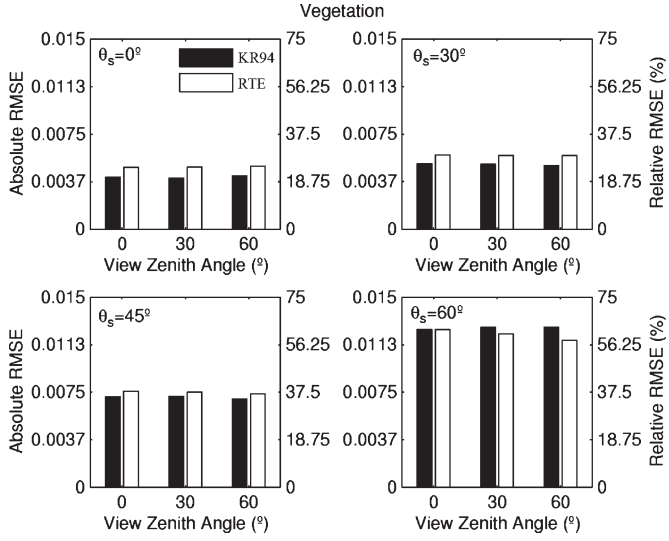

Fig. 26. Same as that in Fig. 22 but for MLW.

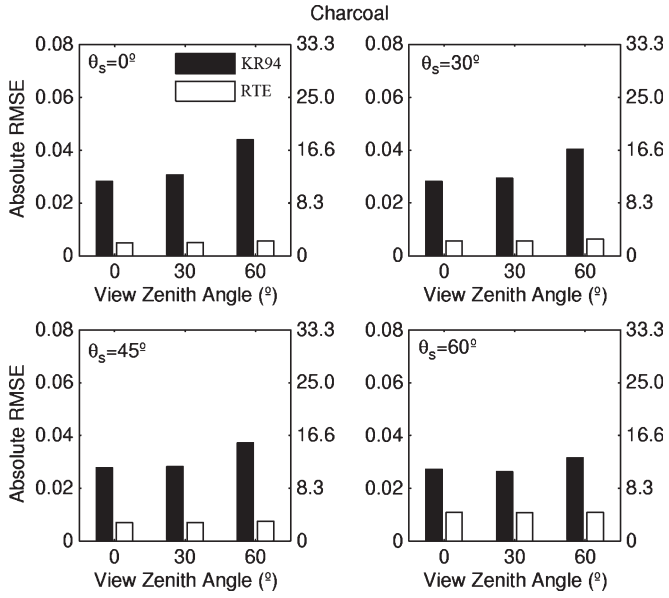

Fig. 27. Same as that in Fig. 26 but for charcoal.

250% (RTE—vegetation) to 18% (RTE—charcoal) in the case of TRO atmosphere and from 38% (KR94—vegetation) to 16% (KR94—charcoal) and from 38% (RTE—vegetation) to 5% (RTE—charcoal) in the case of the MLW atmosphere. These results provide a clear indication that, besides the important role played by moisture (MLW versus TRO), the RTE approach works better than KR94 for virtually all atmospheric conditions and geometries. Nevertheless, an accurate characterization of atmospheric conditions is crucial to ensure appropriate estimates of MIR reflectance.

In the case of low sun elevations (SZA around 60°), the retrieval of MIR reflectance is severely contaminated by errors, particularly for TRO and MLS, and it may be noted that the impact of ill-conditioning is more severe in the case of RTE than when KR94 is used. In fact, even if the retrieved values using KR94 are still unusable for high values of SZA, it is worth stressing that the errors in MIR reflectance are smaller than the corresponding errors when using RTE, which means that the approximations made in the simplified algorithm (i.e., in KR94) tend to smooth the effects of ill-conditioning. This feature may reveal to be useful when attempting to develop an algorithm able to produce usable estimates of MIR reflectance for high values of SZA.

D. Impacts on BA Discrimination

Assessing the impact of errors in retrieved MIR reflectance on BA discrimination by applying RTE or KR94 to real imagery, no matter how attractive it might seem, is always impaired by the virtual absence of "*in situ*" (direct) measurements [30]. A compromise with reality may however be achieved by perturbing a given image where the atmospheric conditions are particularly favorable, due to low values of the water vapor column and a low amount of aerosols [14]. In such case, values of MIR reflectance will be accurately retrieved by means of

either RTE or KR94 and a realistic reference field of reflectance may be generated. Other atmospheric conditions together with other fields of LST may be prescribed and then MODTRAN-4 may be used to produce synthetic values of TOA MIR radiance. Values of MIR reflectivity may be finally retrieved using either KR94 or RTE, and the performance of the two retrieval algorithms assessed by comparing the respective retrieved values with those of the reference field.

Following [14], the selected set of MODIS images covers the large fire event that took place from April 30 to May 12, 2006 and affected the entire area of the Ilha Grande National Park, located between the states of Paraná and Mato Grosso do Sul, Brazil. The reference field of MIR reflectance was generated based on information as acquired/derived on May 12, 2006 by/from the MODIS instrument onboard Aqua. The generation of reference data of MIR reflectance was then achieved via MODTRAN-4 using TOA values of MIR radiance, TIR brightness temperature, atmospheric profiles of temperature and humidity, LST, and SZA. Details about the entire procedure may be found in [14].

A hot tropical environment was imposed on the scene by assuming a TRO atmospheric profile and by adding 20 K to the LST of May 12, 2006. MODTRAN-4 was then used to produce synthetic values of TOA MIR radiance and TIR brightness temperature. Following the steps described in Sections II-B and II-C, values of MIR reflectance were retrieved using the RTE and KR94.

The effectiveness of both algorithms to discriminate between burned and unburned surfaces was finally assessed by studying the statistical distribution of retrieved MIR reflectance when RSE and KR94 are applied over two sets of selected pixels, namely, a first set of 133 burned pixels, hereafter referred to as the burned class, and a second set of 262 pixels that included the remaining land-cover types (namely, green vegetation, crop fields, and water bodies), hereafter referred to as the unburned class. Details about the selection of pixels are given in [14]. Computed statistics include the mean and the SD for the burned and unburned classes, as well as a discrimination index M derived from the previous statistics according to

$$M = \frac{|\mu_b - \mu_u|}{\sigma_b + \sigma_u} \tag{5}$$

where μ_u (μ_b) is the mean value and σ_u (σ_b) is the SD of the unburned (burned) class. As proposed by [11], the discrimination index may be viewed as an estimator of signal-to-noise ratio, the absolute difference between the mean values of the two classes representing the signal (associated to between-group variability) and the sum of the SDs representing noise (associated to within group variability). Values of M larger than one indicate good separability, whereas values smaller than one represent a large degree of overlap between the values associated to the two classes.

Results obtained for M are shown in Table I, together with the mean and SD of unburned and burned samples. As pointed out in [14], the performance of KR94 is very poor in the case of tropical environments due to the increase in systematic and random errors, namely, for the unburned class. There is a shift of μ_u (μ_b) from the reference value of 0.02 (0.11) to 0.17 (0.18), leading to an almost indistinguishability of the two classes in terms of the mean. Such shift is accompanied by an increase in σ_u (σ_b) from the reference value of 0.020 (0.032) to 0.046 (0.033), contributing to a further decrease in M from the reference value of 1.82 to 0.53 that indicates a very poor effective discrimination. In the case of RTE, both increases in μ_u (μ_b) from 0.02 (0.11) to 0.06 (0.15) and in σ_u from 0.020 to 0.032 are much smaller, leading to a decrease in M from 1.82 to 1.30, an indication that discrimination between burned and unburned classes is still possible based on retrieved values of MIR reflectance via RSE.

TABLE I
MEAN VALUE μ_u (μ_b) AND STANDARD DEVIATION σ_u (σ_b) OF UNBURNED (BURNED) CLASSES AND DISCRIMINATION INDEX M FOR REFERENCE AND RETRIEVED VALUES OF SURFACE REFLECTANCE WHEN USING RTE AND KR94 IN THE CASE OF A TROPICAL HOT ATMOSPHERE

	μ_u	σ_u	μ_b	σ_b	M
Reference	0.02	0.020	0.11	0.032	1.82
RTE	0.06	0.032	0.15	0.039	1.30
KR94	0.17	0.046	0.18	0.033	0.53

IV. DISCUSSION AND CONCLUSION

The purpose of this work was twofold: 1) to investigate the problem of retrieving MIR reflectance in MODIS channel 20, namely, when using the full RTE approach, as given by (2) or using the algorithm proposed by Kaufman and Remer [11] (KR94 approach), as given by (3); and 2) to assess the implications of using both methods to retrieve values of MIR reflectance from MODIS imagery in order to discriminate BAs in tropical environments. This second aspect is particularly relevant since major efforts are being devoted to the design of optimal spectral indexes for BA mapping at the regional or global scale [31] and because improvements have been achieved when incorporating in the index the reflective part of MIR [1]–[3], [8].

The measurement errors that may affect the accuracy of the estimated MIR reflectance were first characterized, namely, those associated to the following: 1) the noise in MODIS channels; 2) the errors in the atmospheric profile; and 3) the uncertainties in LST. A sensitivity study was then performed based on a set of conditions closely reflecting those of an operational environment. The effect of errors in the atmospheric profile source was assessed by perturbing three reference profiles (MLW, MLS, and TRO) with values based on the current ECWMF background error covariance matrix. Realistically perturbed values of LST were, in turn, generated based on the errors from the MODIS LST product (MOD11_L2).

For given atmospheric conditions, namely, those that are likely to be encountered in tropical environments, and for certain geometric conditions, namely, high values of SZA, the retrieval of MIR reflectance from radiance measurements based on RTE is an ill-posed problem. The solution does not depend continuously on the data, i.e., small perturbations in measurements (due to, e.g., sensor noise and uncertainties in atmospheric profiles and LST) may induce large errors in the

solution. It is further shown that this problem occurs for the same combinations of pairs of LST and SZA where KR94 does not lead to a proper retrieval of MIR reflectance, as described in [14].

Although in the case of dry and cold atmospheres (e.g., MLW), the increase in performance when using the RTE instead of KR94 is not significant, deviations in favor of RTE are more pronounced for moist and hot atmospheres, like TRO. However, the estimated values of the total error when using RTE point out the need of having accurate atmospheric and LST data, the total error being almost completely driven by the uncertainty on these two parameters.

Results from this work, together with those from [14], allow one to conclude that the RTE approach leads to better estimates of MIR reflectance than those provided by KR94 in virtually all cases, the exception consisting of low sun elevations and high LST, where results from KR94 are also not usable. Results further suggest that there are no advantages in using RTE as a surrogate for KR94 when geometric and atmospheric conditions turn the inversion into an ill-posed problem.

Based on results obtained, an assessment of the impacts when retrieving MIR reflectance for BA discrimination via RTE or KR94 was performed. For this purpose, reference values of MIR reflectance were first derived from MODIS imagery showing a large fire event in southern Brazil. Synthetic values were then generated, assuming a hot tropical environment and MIR reflectance was retrieved via the RTE and KR94 approaches. Whereas the latter approach led to retrieved values of MIR reflectance that do not allow an effective discrimination between burned and unburned areas in hot tropical environments, estimated values obtained via RTE have shown to be usable for BA monitoring.

Despite the better performance of RTE when compared with KR94, particularly in the case of tropical environments, the atmospheric correction and the LST estimation are time consuming and there is the additional problem related to the need of atmospheric and LST data which are not always operationally available and/or accurate. The method developed by Kaufman and Remer [11] presents the advantage of neither requiring any auxiliary data sets (e.g., atmospheric profiles) nor major computational means (e.g., radiative transfer computations). As shown in [14], with the exception of low sun elevations and high LST values, the discrimination between burned and unburned surfaces may be achieved on reasonably good grounds when using estimated values of MIR reflectance via the KR94 approach.

The RTE alternative offers, in turn, good perspectives for BA discrimination in hot tropical environments as well as in all problems (e.g., LST and surface emissivity retrieval) that require precise quantitative values of MIR reflectance.

ACKNOWLEDGMENT

The work of R. Libonati was partially developed at the Satellite Division of the Brazilian National Institute for Space Research (DSA/INPE). The authors would like to thank Dr. A. Setzer (DSA/INPE) for the valuable discussions and suggestions.

REFERENCES

[1] J. M. C. Pereira, "A comparative evaluation of NOAA/AVHRR vegetation indexes for burned surface detection and mapping," *IEEE Trans. Geosci. Remote Sens.*, vol. 37, no. 1, pp. 217–226, Jan. 1999.

[2] D. P. Roy, L. Giglio, J. D. Kendall, and C. O. Justice, "Multi-temporal active-fire based burn scar detection algorithm," *Int. J. Remote Sens.*, vol. 20, no. 5, pp. 1031–1038, 1999.

[3] P. M. Barbosa, J.-M. Gregoire, and J. M. C. Pereira, "An algorithm for extracting burned areas from time series of AVHRR GAC data applied at a continental scale," *Remote Sens. Environ.*, vol. 69, no. 3, pp. 252–263, Sep. 1999.

[4] H. França and A. W. Setzer, "AVHRR analysis of savanna site through a fire season in Brazil," *Int. J. Remote Sens.*, vol. 22, no. 13, pp. 2449–2461, 2001.

[5] T. F. Eck, B. N. Holben, I. Slutsker, and A. Setzer, "Measurements of irradiance attenuation and estimation of aerosol single scattering albedo for biomass burning aerosols in Amazonia," *J. Geophys. Res.*, vol. 103, no. D24, pp. 31 865–31 878, Dec. 1998.

[6] J. M. C. Pereira, "Remote sensing of burned areas in tropical savannas," *Int. J. Wildland Fire*, vol. 12, no. 3/4, pp. 259–270, 2003.

[7] R. Libonati, C. C. DaCamara, J. M. C. Pereira, A. Setzer, and F. Morelli, "A new optimal index for burned area discrimination in satellite imagery," in *Proc. IN EUMETSAT Meteorol. Satellite Conf. 15th Satellite Meteorol. Oceanogr. Conf. Amer. Meteorol. Soc.*, 2007, pp. 1–7.

[8] R. Libonati, C. C. DaCamara, J. M. C. Pereira, and L. F. Peres, "On a new coordinate system for improved discrimination of vegetation and burned areas using MIR/NIR information," *Remote Sens. Environ.*, vol. 115, no. 6, pp. 1464–1477, Jun. 2011.

[9] Z.-L. Li and F. Becker, "Feasibility of land surface temperature and emissivity determination from NOAA/AVHRR data," *Remote Sens. Environ.*, vol. 43, no. 1, pp. 67–85, Jan. 1993.

[10] F. Nerry, F. Petitcolin, and M.-P. Stoll, "Bidirectional reflectivity in AVHRR channel 3: Application to a region in Northern Africa," *Remote Sens. Environ.*, vol. 66, no. 3, pp. 298–316, Dec. 1998.

[11] Y. J. Kaufman and L. Remer, "Detection of forests using mid-IR reflectance: An application for aerosol studies," *IEEE Trans. Geosci. Remote Sens.*, vol. 32, no. 3, pp. 672–683, May 1994.

[12] F. Petitcolin and E. Vermote, "Land surface reflectance, emissivity and temperature from MODIS middle and thermal infrared data," *Remote Sens. Environ.*, vol. 83, no. 1/2, pp. 112–134, Nov. 2002.

[13] S. Trigg and S. Flasse, "An evaluation of different bi-spectral spaces for detecting burned shrub-savannah," *Int. J. Remote Sens.*, vol. 22, no. 13, pp. 2641–2647, 2001.

[14] R. Libonati, C. C. DaCamara, J. M. C. Pereira, and L. F. Peres, "Retrieving middle-infrared reflectance for burned area mapping in tropical environments using MODIS," *Remote Sens. Environ.*, vol. 114, no. 4, pp. 831–843, Apr. 2010.

[15] Air Force Research Laboratory, Space Vehicles Directorate, Air Force Material Command, Hanscom AFB, MA 01731-3010, A. Berk, G. P. Anderson, P. K. Acharya, J. H. Chetwynd, I. S. Bernstein, E. P. Shettle, M. W. Matthew, and S. M. Alder-Golden, MODTRAN4 Version 2 User's Manual.

[16] Z. Wan and J. Dozier, "A generalized split-window algorithm for retrieving land-surface temperature from space," *IEEE Trans. Geosci. Remote Sens.*, vol. 34, no. 4, pp. 892–905, Jul. 1996.

[17] G. Gessel, "An algorithm for snow and ice detection using AVHRR data: An extension to the APOLLO software package," *Int. J. Remote Sens.*, vol. 10, no. 4, pp. 897–905, 1989.

[18] I. Ruff and A. Gruber, "Multispectral identification of clouds and earth surfaces using AVHRR data," in *Proc. 5th Conf. Atmos. Radiat.*, Baltimore, MD, Oct. 31–Nov. 4 pp. 475–478.

[19] S. Trigg and S. Flasse, "Characterizing the spectral–temporal response of burned savannah using in situ spectroradiometry and infrared thermometry," *Int. J. Remote Sens.*, vol. 21, no. 16, pp. 3161–3168, 2000.

[20] A. M. S. Smith and J. A. Sobrino, "Testing the potential of multi-spectral remote sensing for retrospectively estimating fire severity in African Savannahs environments," *Remote Sens. Environ.*, vol. 97, no. 1, pp. 92–115, 2005.

[21] J. C. Jiménez-Muñoz and J. A. Sobrino, "Errors sources on the land surface temperature retrieved from thermal infrared single channel remote sensing data," *Int. J. Remote Sens.*, vol. 27, no. 5, pp. 999–1014, Mar. 2006.

[22] S. A. Tjemkes and J. Schmetz, "Radiative transfer simulations for the thermal channels of METEOSAT second generation," EUMETSAT, Darmstadt, Germany, Tech. Memo. 1, 1998.

[23] L. F. Peres and C. C. DaCamara, "LST and emissivity estimation based on the two-temperature method: sensitivity analysis using simulated MSG/SEVIRI data," *Remote Sens. Environ.*, vol. 91, no. 3/4, pp. 377–389, Jun. 2004.
[24] L. Fillion and J.-F. Mahfouf, "Coupling of moist-convective and stratiform precipitation processes for variational data assimilation," *Monthly Weather Rev.*, vol. 128, no. 1, pp. 109–124, 2000.
[25] D. C. Tobin, H. E. Revercomb, R. O. Knutson, B. M. Lesht, L. L. Strow, S. E. Hannon, W. F. Feltz, L. A. Moy, E. J. Fetzer, and T. S. Cress, "Atmospheric radiation measurement site atmospheric state best estimates for atmospheric infrared sounder temperature and water vapor retrieval validation," *J. Geophys. Res.*, vol. 111, p. D09 S14, 2006.
[26] Z. Wan, MODIS land-surface temperature algorithm theoretical basis document (LST ATBD): Version 3.3, Univ. California, Santa Barbara, CA. [Online]. Available: http://www.icess.ucsb.edu/modis/atbd-mod-11.pdf
[27] C. D. Rodgers, *Inverse Methods for Atmospheric Sounding: Theory and Practice*, vol. 2. Singapore: World Scientific, 2000, ser. Atmospheric, Oceanic and Planetary Physics, pp. 1–11.
[28] G.-M. Jiang, Z.-L. Li, and F. Nerry, "Land surface emissivity retrieval from combined mid-infrared and thermal infrared data of MSG-SEVIRI," *Remote Sens. Environ.*, vol. 105, no. 4, pp. 326–340, Dec. 2006.
[29] L. F. Peres and C. C. DaCamara, "Improving two-temperature method retrievals based on a nonlinear optimization approach," *IEEE Geosci. Remote Sens. Lett.*, vol. 3, no. 2, pp. 232–236, Apr. 2006.
[30] J. C. Roger and E. F. Vermote, "A method to retrieve the reflectivity signature at 3.75 mm from AVHRR data," *Remote Sens. Environ.*, vol. 64, pp. 103–114, 1998.
[31] D. Stroppiana, M. Boschetti, P. Zaffaroni, and P. A. Brivio, "Analysis and interpretation of spectral indices for soft multicriteria burned-area mapping in mediterranean regions," *IEEE Geosci. Remote Sens. Lett.*, vol. 6, no. 3, pp. 499–503, Jul. 2009.

Renata Libonati received the B.S. and Ph.D. degrees in geophysics from the University of Lisbon, Lisbon, Portugal, in 2005 and 2011, respectively. Her Ph.D. work was partially developed at the Satellite Division, Brazilian National Institute for Space Research (DSA/INPE).

She has been doing active research in remote sensing of surface parameters within the framework of several European research projects. She is currently part of the research team of the Instituto Dom Luiz, University of Lisbon. Her recent work focuses on the development and validation of remote sensing algorithms for burned area mapping at regional and global scales.

Carlos C. DaCamara received the Ph.D. degree in atmospheric science from the University of Missouri, Columbia, in 1991.

He is currently an Associate Professor with the Faculty of Sciences, University of Lisbon, Lisbon, Portugal, where he is part of the research team of the Instituto Dom Luiz. From May 2003 to April 2004, he was Vice President of the Instituto de Meteorologia, the Portuguese national meteorological service. He was the Scientific Coordinator of the Land Surface Analysis Satellite Application Facility, an R&D Project supported by EUMETSAT, since its beginning in 1999 until December 2005. He has been doing research in climatic variability and climate change, namely, with respect to exploring relationships between atmospheric circulation types and large fire events.

José Miguel C. Pereira received the B.S. degree in forestry from the Instituto Superior de Agronomia, Universidade Técnica de Lisboa, Lisbon, Portugal, in 1983 and the Ph.D. degree in renewable natural resources studies from The University of Arizona, Tucson, in 1989.

He is a Full Professor with the Department of Forestry, School of Agriculture, Technical University of Lisbon, teaching courses in vegetation fires, forest ecology, and remote sensing. His current research interests include the geographical ecology of wildfires in southern Europe and the development of remote sensing algorithms for burned-area mapping at regional and global scales.

Leonardo F. Peres received the B.S. degree in meteorology from the Federal University of Rio de Janeiro, Rio de Janeiro, Brazil, in 1999 and the Ph.D. degree in geophysics from the University of Lisbon, Lisbon, Portugal, in 2005.

Between 2000 and 2005, he was a Research Assistant with the Instituto de Ciência Aplicada e Tecnologia, Lisbon, where he investigated the use of Meteosat Second Generation data to retrieve land-surface temperature and emissivity within the framework of the Satellite Application Facility on Land Surface Analysis, which is supported by EUMETSAT. From 2005 to 2009, he was part of the research team of the Instituto Nacional de Pesquisas Espaciais, Centro de Previsão de Tempo e Estudos Climáticos, Cachoeira Paulista, SP, Brazil. His current research interests include the retrieval of emissivity and surface temperature from satellite data. Since 2009, he is an Assistant Professor with the Department of Meteorology, Federal University of Rio de Janeiro, Brazil.